Electronic Properties of Large Metal Clusters in Jellium and Pseudo-Jellium Models

F. Catara
Dipartimento di Fisica, Università di Catania
and INFN, Sezione di Catania, I-95129 Catania, Italy
e-mail: CATARA@CATANIA.INFN.IT

Ph. Chomaz
Grand Accélérateur National d'Ions Lourds
B.P. 5027, F-14021 Caen Cedex, France
e-mail: CHOMAZ@GANAC4.IN2P3.FR

N. Van Giai
Division de Physique Théorique, Insitut de Physique Nucléaire,
F-91406 Orsay Cedex, France
e-mail: NGUYEN@IPNCLS.IN2P3.FR

GANIL P 94 27

Electronic Properties of Large Metal Clusters in Jellium and Pseudo-Jellium Models

F. Catara
Dipartimento di Fisica, Università di Catania
and INFN, Sezione di Catania, I-95129 Catania, Italy
e-mail: CATARA@CATANIA.INFN.IT

Ph. Chomaz
Grand Accélérateur National d'Ions Lourds
B.P. 5027, F-14021 Caen Cedex, France
e-mail: CHOMAZ@GANAC4.IN2P3.FR

N. Van Giai
Division de Physique Théorique, Insitut de Physique Nucléaire,
F-91406 Orsay Cedex, France
e-mail: NGUYEN@IPNCLS.IN2P3.FR

Abstract

The energy-density functional approach and jellium-like models are used to examine two important electronic properties of metal (Li, Na, K) clusters: their shell and supershell structures, and the behaviour of plasmon energies with increasing cluster sizes. A comparative study is made between predictions of the usual jellium model and those of the pseudo-jellium model where pseudo-hamiltonians are used.

PACS numbers: 36.40+d, 31.20.Sy, 71.45.Gm

IPNO/TH 94-62 August 1994

1 Introduction

Metal clusters are a unique laboratory to study the properties of very large finite Fermi systems. The experimentally observed [1, 2, 3, 4, 5] persistency of shell effects in clusters up to several thousand atoms is an example of phenomena whose investigation has become possible. To date, the most complete microscopic theoretical study of shell effects in large metal clusters is that of Ref. [6] , where the Kohn-Sham (KS) method based on the jellium model (JM) was used to analyze the supershell structure of systems up to 3000 atoms.

Another interesting feature of metal clusters is that they show a prominent peak in the optical response spectrum. This collective plasmon resonance, reminiscent of the well known nuclear giant dipole resonance, has been observed in metal clusters up to a few thousand atoms [7]. Time Dependent Local Density Approximation (TDLDA) calculations based on the jellium model are able to describe the qualitative behaviour of the peak energy as a function of the cluster size, in particular the fact that for large metal clusters its position tends to a finite value. However, the TDLDA energy turns out to be appreciably higher than the experimental value in some cases. For instance, in Li clusters the difference is 30 %. In Ref. [8] this discrepancy was remedied by using ionic pseudo-hamiltonians [9], which effectively take into account the influence of core electrons on the dynamics of the valence ones, to build a jellium-like model which the authors named pseudo-jellium (PJM).

The aim of the present paper is twofold. On one hand, we want to see how much the magic numbers obtained in Ref. [6] within the JM are different from those calculated within the PJM . On the other hand, we want to complete the investigation of Ref. [8] by calculating the TDLDA excitation spectrum for very large metallic clusters in order to determine the limiting value of the peak energy of the collective plasmon resonance. As it is well known [10], in nuclei the energy of the giant dipole resonance decreases as $A^{-1/3}$ with increasing mass number A and this behaviour is quite well reproduced by TDLDA. It is thus interesting to see that TDLDA is also able to give the correct size dependence of the plasmon resonance energy whose limit for large clusters is a non-zero value. This different behaviour can be ascribed to the very different range of the force in the two cases : short in nuclei and very long in metal clusters.

Many experimental data on metal clusters and various theoretical approaches used to study them are reported and described in two recent review papers [11, 12] where a quite complete bibliography on the subject can be found. Therefore we will refer to [12] for details on the jellium model, the Kohn-Sham method and the TDLDA approximation. The pseudo-jellium model is illustrated in Ref. [8] , where it was introduced. All calculations in the present work are done for neutral clusters.

2 Shell effects in very large metal clusters

The first systematic theoretical study of shell closures in very large metal clusters was done [13] by introducing a simple parametrization, in terms of a Woods-Saxon (WS) potential, of the mean field in which the valence electrons move. This allowed to predict the existence of supershells in metal clusters up to $\sim$ 4000 atoms. A completely microscopic study of the same phenomenon within the jellium model was reported in Ref. [6], where the Kohn-Sham

equations were solved for Na clusters up to $\sim$ 3000 atoms.

As we said before, one of the aims of the present paper is to perform a similar analysis within the pseudo-jellium model [8] which has been shown to be able to remedy the discrepancy, observed especially for Li clusters, between the experimental peak energy of the plasmon resonance and the theoretical result obtained by using the TDLDA based on the JM. The essential point of the PJM is that a pseudo-hamiltonian is introduced to take into account the influence of core electrons on the dynamics of valence ones [9].

The KS equations are usually solved by iteration, starting from a given sequence of occupied single-particle (s.p.) states. For large cluster sizes the level density is large, thus the energy difference between the highest occupied s.p. level (HOMO) and the lowest unoccupied one (LUMO) is small. This may introduce some instability in the ordering of the levels around the Fermi surface, before the convergence of the iterative procedure is reached. Therefore it is important to have a reasonable zeroth order approximation for the sequence of occupied s.p. levels. The presence in the pseudo-hamiltonian of an effective mass and of angular momentum dependent terms makes this problem even worse in the PJM. In order to perform KS calculations for very large clusters, we have exploited a step by step procedure making use of a WS parametrization of the mean field to get a zeroth order approximation, which is then used as a starting point for the solution of the KS equations. To be more precise, the procedure is as follows:

1) perform KS calculations for a few not very large (N $\leq$ 1000) closed-shell clusters. For such sizes the sequence of levels in an infinite square well is a good starting point.

2) find the best values of the parameters of the WS potential by fitting the previously determined s.p. energies. The radius of the potential is taken as $R = r_0 N^{1/3}$. The parameters of the fit are the radius r_0, the diffusivity a and the depth V_0 of the WS potential.

3) use this potential to make a guess for a larger magic number. The criterion used to decide on a shell closure is to look at the LUMO-HOMO energy gap: a magic number should correspond to a larger value of that gap. We will discuss this point later on.

4) perform a KS calculation for that cluster. If the results of such microscopic calculation confirm the occurrence of a shell closure, the procedure is iterated starting from point 2), including also the s.p. energies of the just considered larger cluster. In our calculations we have included clusters of sizes N$\sim$ 1000, 2000, 3000, 4000 in order to determine the best WS potential.

In the case of PJM calculations a parametrization of the effective mass is also needed. Guided by the results of Ref. [8], we have expressed it as

$$\frac{m^*(r)}{m} = 1 + \frac{\Delta_m}{1 + exp((r - R_m)/a_m))} , \tag{1}$$

with

$$R_m = r_m N^{1/3} . \tag{2}$$

The parameters Δ_m, r_m and a_m are fitted to the microscopically calculated effective mass for a large set of cluster sizes. This parametrization has been used only in conjunction with the use of the WS potential for the mean field. In Table 1 we report the parameters entering in the potential and in the effective mass. The WS potential parametrizing the mean field turns out to have a smaller depth and a larger diffusivity in the PJM than in the JM, while the radius is almost the same in the two models. The effective mass in Li clusters is somewhat larger than 1, while in Na it is only a little larger than 1, and a little less than 1 in K.

By using the above described procedure we have performed calculations for K, Li and Na clusters up to $\sim$ 5500 atoms, both in the jellium and in the pseudo-jellium models. We have used the energy functional of Ref. [14]. The KS equations have been solved in a box of radius equal to $\sim$ 1.5 times the radius of the clusters. The stability of the results against small variations of the box size has been tested. The Wigner-Seitz radius r_s has been taken equal to 4.86, 3.26 and 3.93 a.u. for K, Li and Na, respectively. The quality of the fit obtained for the s.p. energies can be appreciated from Figs. 1 and 2, where for some large clusters we show the KS s.p. energies of occupied orbitals (solid line) and those obtained by using the WS potential (dashed line). The numbers in the abscissa just indicate the order of the levels. In Fig.3 we report the s.p. energies of Na_{3028} obtained with the WS potential of Ref. [13] (dashed line) as compared with those resulting from our WS and from the KS calculations within JM (the two solid lines). As it is apparent, our procedure gives a WS potential whose s.p. energies are in a much better agreement with those obtained by solving the KS equations.

Let us now come to the problem of the identification of shell closures. One possibility is to divide the total energy E in a smooth part $\bar{E}$ and a fluctuating one δE. The smooth part can be calculated by fitting E with a Liquid Drop (LD) expansion [6, 12]. A shell closure will correspond to a negative peak in the shell correction energy

$$\delta E \;=\; E - \bar{E}\,. \tag{3}$$

This procedure, however, requires a rather big computational effort because one should determine the total energy for a large set of cluster sizes. The numerical effort could be drastically reduced by replacing in the above procedure the total energy with the sum of the s.p. energies in the WS potential introduced to parametrize the mean field. This method has been used in Ref. [13] to predict the magic numbers in Na clusters up to N $\sim$ 4000. The existence of supershells was also beautifully put in evidence. This method, however, presents some drawbacks. First of all, the sum of the s.p. energies provides a crude approximation to the total energy. In as much as the determination of the shell energy is concerned, the method may nevertheless give reasonable results. Indeed, the difference between the total energy and the sum of the s.p. energies should be a smooth function of N, while δE is defined as the deviation of the total energy from its smooth interpolation performed by means of a LD expansion. Another problem is related to the fact that the shell energy is of the order of a few eV, while the total energy ranges from a few tens eV for small clusters, to several thousands eV for large ones. Thus, when using the same LD parametrization of $\bar{E}$ for all sizes, one may expect some ambiguities for small clusters.

A more direct approach, closely related to how the magic numbers are experimentally observed, is to look at the ionization potentials (IP). As it is well known, a signature of a major shell closure at some N is a sudden large increase of $\Delta IP(N) = IP(N) - IP(N+1)$. The closure of a subshell corresponds to a less pronounced peak in $IP(N)$. Many experiments [5] aimed at the determination of magic numbers in metal clusters are based on the same point of view. Now, apart from some rearrangement terms, $IP(N)$ is approximately equal to $-\varepsilon_{HOMO}$, i.e., the energy of the highest occupied s.p. level, while $IP(N+1) \simeq -\varepsilon_{LUMO}$, i.e., the energy of the lowest unoccupied s.p. level in the cluster with N electrons. Therefore, to a good approximation

$$\Delta IP(N) \simeq \Delta\varepsilon(N) , \tag{4}$$

where

$$\Delta\varepsilon(N) \equiv \varepsilon_{LUMO}(N) - \varepsilon_{HOMO}(N) . \tag{5}$$

We have checked numerically the relation (4) by comparing the $\Delta IP(N)$ and $\Delta\varepsilon(N)$ obtained by solving the KS equations in several cases for neutral Li clusters within the JM. The results are reported in Table 2 and show a strong correlation in the behaviour of $\Delta IP(N)$ and $\Delta\varepsilon(N)$. Namely, both quantities point out N=58 as corresponding to the closure of a major shell. Therefore the criterion we have adopted to determine the magic numbers is to look at $\Delta\varepsilon(N)$. On the other hand, as previously shown in Figs.1-3, the s.p. energies in our WS potential are almost identical to those obtained by solving the KS equations, especially for the large cluster sizes in which we are interested. Therefore, we have used the $\Delta\varepsilon(N)$ determined from the WS potential.

In Fig.4 we show the so calculated differences $\Delta\varepsilon(N)$ for neutral Li clusters of sizes ranging from ~200 to ~6000 atoms. In the lower part of the figure the $\Delta\varepsilon(N)$ obtained within the PJM are shown as vertical bars. One clearly sees two sequences of lines. One, equispaced in the plot as a function of $N^{1/3}$, corresponds to the closure of major shells. The other sequence corresponds to subshell closures. In order to better visualize the major shells we also show the curve obtained by folding the discrete distribution with a gaussian in the variable $x = N^{1/3}$. The width of the gaussian is 0.05. In the middle part of the figure we report the results obtained in the JM. In the upper part, finally, we compare the results in the two models. Apart from some shifts in the position of the maxima, more important for N≥3000 , the main feature is an almost uniform scaling of the heights of the peaks. Namely, the peaks resulting from the PJM calculations are lower than the JM ones by a factor very close to the effective mass of valence electrons in the interior region of the cluster, i.e., a factor ~ 1.5 . This can be related to the fact that the level spacing in a potential is inversely proportional to the mass. As shown in Figs.5 and 6, the differences between JM and PJM are much smaller in the cases of Na and K clusters, in accordance with the fact that $m^*(0)$ =1.04 for Na and 0.98 for K. It is also interesting to compare the results between clusters made of different atoms. In Fig.7 we show the smoothed $\Delta\varepsilon(N)$

as a function of $N^{1/3}$ for Li (thin line) and Na (thick line) in the JM (upper panel) and PJM (lower panel). The two curves in the latter model are almost identical. Since the only two quantities characterizing the clusters are the Wigner-Seitz radius and the effective mass, this means that the effects of the smaller radius of Li clusters are compensated by the larger effective mass. This can be qualitatively understood since one expects that a smaller radius gives a larger level spacing, while a larger effective mass reduces it. For example, in a square well potential the level spacing is inversely proportional to mR^2. As shown in Fig.8, the same effect is seen when Li (thin curve) and K (thick curve) are compared. In this case, however, the compensation is not as perfect as in the previous one. This is related to the fact the radii of K and Na are ~ 1.5 and ~ 1.22 times that of Li, respectively, while their effective masses are almost equal.

To complete our analysis, we have also studied the shell closures by using the procedure of Ref. [13], i.e., by looking at the shell correction energy. The results for Na clusters in PJM are shown in the upper panel of Fig.9 . By comparing with the lower panel of Fig.5 we see that the two procedures give very similar predictions as far as the location of the major shells is concerned. The expected beating pattern between two shell sequences, usually called supershell effect is also observed. A similar pattern arises also from our previous analysis, based on the maxima of the ΔIP at the shell closures. Indeed, by folding the discrete distribution of bars in Fig.5 with a gaussian having a width smaller than the spacing of major shells, but larger than the spacing of subshells, one gets the curve drawn in the lower panel of Fig.9 . The positions of the maxima of the lower curve very closely correspond to the minima of the upper one. In particular, both curves have nodes at $N^{1/3} \simeq 10$ and 16. As shown in Fig.10, in the case of Li clusters the positions of the nodes as obtained in JM (upper curve) and PJM (lower curve) are somewhat different. The difference is more pronounced for large masses: the JM calculations predict a node at $N^{1/3} \simeq 16$ (N$\simeq$ 4000) while within the PJM we get a node at $N^{1/3} \simeq 17$ (N $\simeq$ 4900). Similar results are also found for K and Na clusters, but the shift is much smaller there.

3 TDLDA calculations of plasmon resonance energies

The peak energy of the collective plasmon resonance observed in Li clusters up to N=1500 atoms, extrapolated to $N \rightarrow \infty$,tends to the value 3.55 eV [7]. This value is in excellent agreement with the surface plasmon energy of a macroscopic metallic sphere deduced from the measured macroscopic dielectric constant of Li, 3.55 ± 0.1 eV. TDLDA calculations based on the JM fail to reproduce this limit, the extrapolated theoretical value being 4.62 eV. In Ref. [8] it was shown that calculations based on the PJM give results in quite good agreement with the experiment up to N=440. In the present paper we extend such calculations up to N $\sim$ 5500 in order to get a good extrapolation of the theoretical results for $N \rightarrow \infty$. Since the KS equations have been solved by imposing box boundary conditions, the particle-hole (p-h) configuration space is discrete but infinite. Thus, it must be truncated for practical purposes. In doing so, a criterion to be fulfilled is that the f-sum rule must be exhausted to a good accuracy. We have introduced a cutoff based on the f-sum rule, namely we have considered only the p-h configurations contributing more than

a chosen cutoff value to the f-sum rule. In this way, by excluding the p-h configurations contributing less than 10^{-5} of the total f-sum rule, we have constructed a space of ~ 500 p-h configurations for N $\sim$ 5500 and obtained an accuracy better than 1 % in the f-sum rule.

In Table 3 the peak energy E_{peak} of the collective plasmon for K, Li and Na, within both JM and PJM, are reported for several cluster sizes. The introduction of the pseudo-hamiltonian gives rise to a lowering of the resonance peak. In the Li case, due to its larger effective mass, the corrections are quite important. For example, the PJM energy for N $\sim$ 1500 is $\sim$ 1 eV lower than the JM one and it is in reasonable agreement with the experimental value of 3.25 eV [7].

In order to understand qualitatively the behaviour of the plasmon resonance energy as a function of the cluster size N, let us consider the k-th energy weighted moment of the strength distribution

$$M_k^{(\lambda)} = \sum_n (E_{n\lambda})^k |\langle n\lambda|O_\lambda|0\rangle|^2 , \tag{6}$$

where O_λ is the λ-multipole of a given one-body operator, in our case the electromagnetic transition operator, and $E_{n\lambda}$ and $|n\lambda\rangle$ the eigenvalues and eigenvectors of the system under study. In these notations the f-sum rule corresponds to $M_{k=1}^{(\lambda=1)}$. An estimate of the peak energy (in fact an upper bound) can be obtained as [12, 15]

$$\bar{E}_\lambda = \left(\frac{M_3^{(\lambda)}}{M_1^{(\lambda)}}\right)^{\frac{1}{2}} . \tag{7}$$

In the case of a dipole transition and within the JM one gets [16]

$$M_1^{(1)}(JM) = \frac{1}{2}N , \tag{8}$$

and

$$M_3^{(1)}(JM) = \frac{1}{2}N_{ions}\omega_{Mie}^2 , \tag{9}$$

where $\omega_{Mie} = r_s^{-3/2}$ is the so called Mie frequency, i.e., the surface plasmon energy of a macroscopic metallic sphere, and

$$N_{ins} = \int_{r\leq R} \rho(r) d^3r \tag{10}$$

$$= \int \rho(r) d^3r - \int_{r\geq R} \rho(r) d^3r \tag{11}$$

$$\equiv N - \Delta N \,, \tag{12}$$

is the number of electrons inside the jellium radius, ΔN being the electronic spillout. Thus, one has

$$\bar{E}_1^{JM} = \omega_{Mie}\left(1 - \frac{\Delta N}{N}\right)^{\frac{1}{2}} \,,$$

$$\simeq \omega_{Mie}\left(1 - c^{(JM)} N^{-\frac{1}{3}}\right) \,, \tag{13}$$

which, in the limit of large N, gives ω_{Mie}. To calculate the electronic spillout ΔN, only the density outside the jellium sphere is required. Thus, its oscillations in the interior part can be disregarded and one may try to fit it with a WS shape. We find that, for large clusters, the parameters of the WS function obtained by separately fitting the densities resulting from KS calculations for several values of N are independent of N. In particular, by defining the radius of the WS as $R = r_d N^{1/3}$, it turns out that $r_d = r_s$ within less than 1 %. The so obtained values of r_d and diffusivity a_d are reported in Table 4. The depth of the WS form was fixed by normalizing it to the number of electrons. The only difference in going from JM to PJM is an increase of the diffusity in the latter model. By integrating the WS fitted density outside the jellium radius one easily gets that the leading term in the electronic spillout is proportional to R^2, i.e., to $N^{2/3}$. Therefore, the shift of $\bar{E}_1^{JM}$ with respect to ω_{Mie} goes as $N^{-1/3}$.

In the case of PJM the relation (13) is not valid because of the presence of the effective mass and because the pseudo-potential is different from Coulomb inside the cluster. For very large clusters the radius of the effective mass distribution is much larger than its diffusivity, i.e., the extension of the region in which m^* goes rapidly to its bare value. In such cases a relation similar to Eq.(13) can be derived also in PJM[16], namely

$$\bar{E}_1^{PJM} \simeq \omega_{Mie}\left(\frac{m}{m^*_\infty}\right)^{\frac{1}{2}}\left(1 - \frac{\Delta N}{N}\right)^{\frac{1}{2}} \tag{14}$$

$$\simeq \omega_{Mie}\left(\frac{m}{m^*_\infty}\right)^{\frac{1}{2}}\left(1 - c^{(PJM)} N^{-\frac{1}{3}}\right) \,, \tag{15}$$

where m^*_∞ is the effective mass in the bulk. By fitting the " slope parameter " c to the values of E_{peak} shown in the fifth column of Table 3 one gets the values reported in the last column of the same Table. The quite good agreement shows that the parametrization

of Eq.(15) is valid for large cluster sizes. The values of $c^{(JM)}$ and $c^{(PJM)}$, together with the asymptotic values of $\bar{E}_1^{JM}$ and $\bar{E}_1^{PJM}$ are shown in Table 5. In all the 3 considered cases, the slope is much larger in the PJM than in the JM. This fact is related to the larger diffusivity of the electron density in PJM and it explains how, in the case of K clusters, it can happen that for finite sizes the JM peak energy is larger than the PJM value (see Table 3) while in the infinite limit the PJM value becomes slightly larger than the JM value. In Ref. [7] an experimental value of 3.55 eV for E_{peak} extrapolated to $N \rightarrow \infty$ in Li clusters was reported. The introduction of the pseudo-hamiltonian strongly lowers the TDLDA value in Li clusters, bringing it down from 4.62 eV in JM to 3.76 eV in PJM. The change is less marked in Na and K clusters.

4 Conclusion

We have examined in the framework of jellium-like models the electronic properties of metal clusters of sizes ranging from a few hundreds up to a few thousands atoms. We have focussed on two important properties of these systems: the persistence of shell and supershell effects up to very large sizes, and the evolution of plasmon frequencies as the sizes increase. Another goal of this study is to compare the predictions of the usual jellium model with those of the pseudo-jellium model where pseudo-hamiltonians are used.

Although in the energy functional approach where LDA is assumed, the KS energies $|\varepsilon_{HOMO}|$ and $|\varepsilon_{LUMO}|$ cannot be identified to $IP(N)$ and $IP(N+1)$, we have shown that there is a close correlation between $\Delta IP(N)$ and $\Delta\varepsilon(N)$ and therefore, $\Delta\varepsilon(N)$ is a useful (and easy to calculate) quantity for determining shell closures. We also find that our criterion based on $\Delta\varepsilon(N)$ leads to the same magic numbers as the criterion of shell correction energy δE of Ref.[13]. We confirm that electronic supershells appear in Li, Na, and K clusters in the size range N $\sim$ 1000 to 6000. However, the supershell closures predicted by PJM in Li clusters are somewhat shifted to those of JM. For Na and K clusters, the shifts are much smaller.

Concerning the plasmon frequencies, we have found by performing TDLDA calculations in large clusters that the plasmon excitation energies follow closely a linear function of $N^{-1/3}$. By studying the quantity $\bar{E}_1$ defined in terms of energy-weighted sum rules one can easily see that the slope and the value at origin of the functions $\bar{E}_1(N^{-1/3})$ only depend on the electronic spillout and the effective mass m^* (and of course on the Wigner-Seitz radius r_s). The PJM generally gives plasmon energies in better agreement with experiment than the JM. The remaining discrepancies may indicate the limitations of jellium-like models.

Acknowledgements

One of the authors (F.C.) gratefully acknowledges the hospitality and the financial support from the Division de Physique Théorique of IPN-Orsay and from GANIL, where this work has been carried out. This work has been partially supported by the European Community within the programme " Human Capital and Mobility " , contract number CHRX-CT92-0075.

References

[1] Goehlich,H., Lange,T., Bergmann,T., Martin,T.P.: Phys. Rev. Lett. **65**, 748 (1990).

[2] Martin,T.P.,Bergmann,T., Goehlich,H., Lange,T.: Chem. Phys. Lett. **172**, 209 (1990).

[3] Pedersen,J. et al.: Nature (London) **353**, 733 (1991).

[4] Martin,T.P. et al.: Chem. Phys. Lett. **186**, 53 (1991).

[5] Bréchignac,C. et al.: Phys. Rev. **B47**, 2271 (1993-II) and references therein.

[6] Genzken,O., Brack,M.: Phys. Rev. Lett. **67**, 3286 (1991).

[7] Bréchignac,C. et al.: Phys. Rev. Lett. **70**, 2036 (1993).

[8] Serra,Ll., Bachelet,G.B., Van Giai,N., Lipparini,E.: Phys. Rev. **B48**, 14708 (1993-I).

[9] Bachelet,G.B., Ceperley,D.M., Chiocchetti,M.G.B.: Phys. Rev. Lett. **62**, 2088 (1989).

[10] Bohr,A., Mottelson,B.R.: Nuclear Structure, New York: Benjamin 1975.

[11] de Heer,W.A.: Rev. Mod. Phys. **65**, 611 (1993).

[12] Brack,M.: Rev. Mod. Phys. **65**, 677 (1993).

[13] Nishioka,H., Hansen,K., Mottelson,B.R.: Phys. Rev. **B42**, 9377 (1990-II).

[14] Gunnarsson,O., Lundqvist,B.I.: Phys. Rev. **B13**, 4274 (1976).

[15] Lipparini,E., Stringari,S.: Phys. Reports **175**, 103 (1989).

[16] Serra,Ll., Lipparini,E., Van Giai,N., to appear in Phys. Reports.

Table captions

Table 1: Parameters of WS potentials fitted to reproduce Kohn-Sham levels. The constants entering the effective mass parametrization (1) are also shown.

Table 2: Comparison of ΔIP (Eq.(4)) and $\Delta\epsilon$ (Eq.(5)) for some Li clusters.

Table 3: JM and PJM plasmon energies (in eV) for various clusters. E_{peak} and $\bar{E}_1$ are explained in the text.

Table 4: Parameters of the radial shapes of electronic densities fitted to the Kohn-Sham results.

Table 5: JM and PJM slope parameters c and limiting energies in eV (see eq. (13) and (15)).

Figure captions

Figure 1: Energies (in eV) of the occupied s.p. levels of Na_{4154} in the PJM. Solid line: results of KS calculation. Dashed line: results of the WS parametrization. In the abscissa an index ordering the levels is indicated.

Figure 2: Same as in Fig. 1, for Li_{4154}.

Figure 3: Energies (in eV) of the occupied s.p. levels of Na_{3028}. The abscissa has the same meaning as in Figs. 1-2. Dashed line: results of the WS parametrization of Ref. [13]. Solid lines: our WS parametrization and KS results in the JM.

Figure 4: In the lower panel, the vertical bars indicate $\Delta\varepsilon(N)$ (in eV) for Li clusters in the PJM. In the abscissa, $x = N^{1/3}$. The curve has been obtained by folding the bars with a gaussian of width 0.05 in x and dividing by 7 for convenience. In the middle panel, the same but in the JM. In the upper panel, comparison of JM (thin line) and PJM (thick line) results.

Figure 5: Same as in Fig. 4, for Na clusters.

Figure 6: Same as in Fig. 4, for K clusters.

Figure 7: Comparison of the folded $\Delta\varepsilon(N)$ (in eV) in Li (thin line) and Na (thick line) clusters, normalized as in Fig. 4. Lower panel, in the PJM. Upper panel, in the JM. The abscissa is $x = N^{1/3}$.

Figure 8: Same as in Fig. 7, for Li (thin line) and K (thick line) clusters.

Figure 9: In the upper panel, shell correction energy δE (in eV) as a function of $x = N^{1/3}$ for Na clusters in the PJM. In the lower panel, the corresponding $\Delta\varepsilon(N)$ folded with a gaussian of width 0.10 in x. Note that here the $\Delta\varepsilon$ are given in eV.

Figure 10: $\Delta\varepsilon(N)$ (in eV) as a function of $x = N^{1/3}$ folded with a gaussian of width 0.10 in x, for Li clusters. In the upper panel the results in the JM, in the lower panel in the PJM. The normalization is the same as in Fig. 4.

	WS potential			Eff. mass		
	V_0 [eV]	r_0 [a.u.]	a [a.u.]	Δm	r_m [a.u.]	a_m [a.u.]
Li (JM)	-8.02	3.34	0.65			
Na (JM)	-6.26	4.01	0.50			
K (JM)	-3.50	4.96	0.50			
Li (PJM)	-5.98	3.44	0.89	0.512	3.22	0.68
Na (PJM)	-5.71	4.09	1.27	0.036	3.94	0.32
K (PJM)	-3.19	5.07	1.49	-0.019	4.79	0.14

Table 1

Z	$\Delta IP[eV]$	$\Delta\varepsilon[eV]$
40	0.331	0.386
58	0.669	0.683
68	0.073	0.110

Table 2

JM			PJM		
N	E_{peak}	$\bar{E}_1^{JM}$	N	E_{peak}	$\bar{E}_1^{PJM}$
		Li			
1502	4.45	4.51	1314	3.49	3.55
2654	4.54	4.53	2048	3.57	3.58
3028	4.55	4.53	3050	3.64	3.60
4074	4.56	4.54	4154	3.65	3.62
5470	4.57	4.55	5500	3.66	3.63
		Na			
1314	3.36	3.38	1314	3.20	3.20
1502	3.38	3.39	2048	3.22	3.23
2654	3.41	3.41	3028	3.25	3.26
4074	3.44	3.42	4154	3.29	3.27
5470	3.45	3.43	5470	3.30	3.29
		K			
912	2.45	2.48	832	2.24	2.33
2018	2.49	2.49	2018	2.40	2.39
2998	2.51	2.50	3028	2.44	2.41
3848	2.52	2.50	3848	2.46	2.42
5568	2.53	2.51	5108	2.49	2.43

Table 3

cluster	model	r_d[a.u.]	a_d[a.u.]
Li	JM	3.25	0.72
	PJM	3.24	0.93
Na	JM	3.91	0.77
	PJM	3.91	1.14
K	JM	4.83	0.84
	PJM	4.83	1.45

Table 4

cluster	model	c	E_∞
Li	JM	-0.28	4.62
	PJM	-0.60	3.76
Na	JM	-0.33	3.49
	PJM	-0.73	3.43
K	JM	-0.23	2.54
	PJM	-0.87	2.56

Table 5

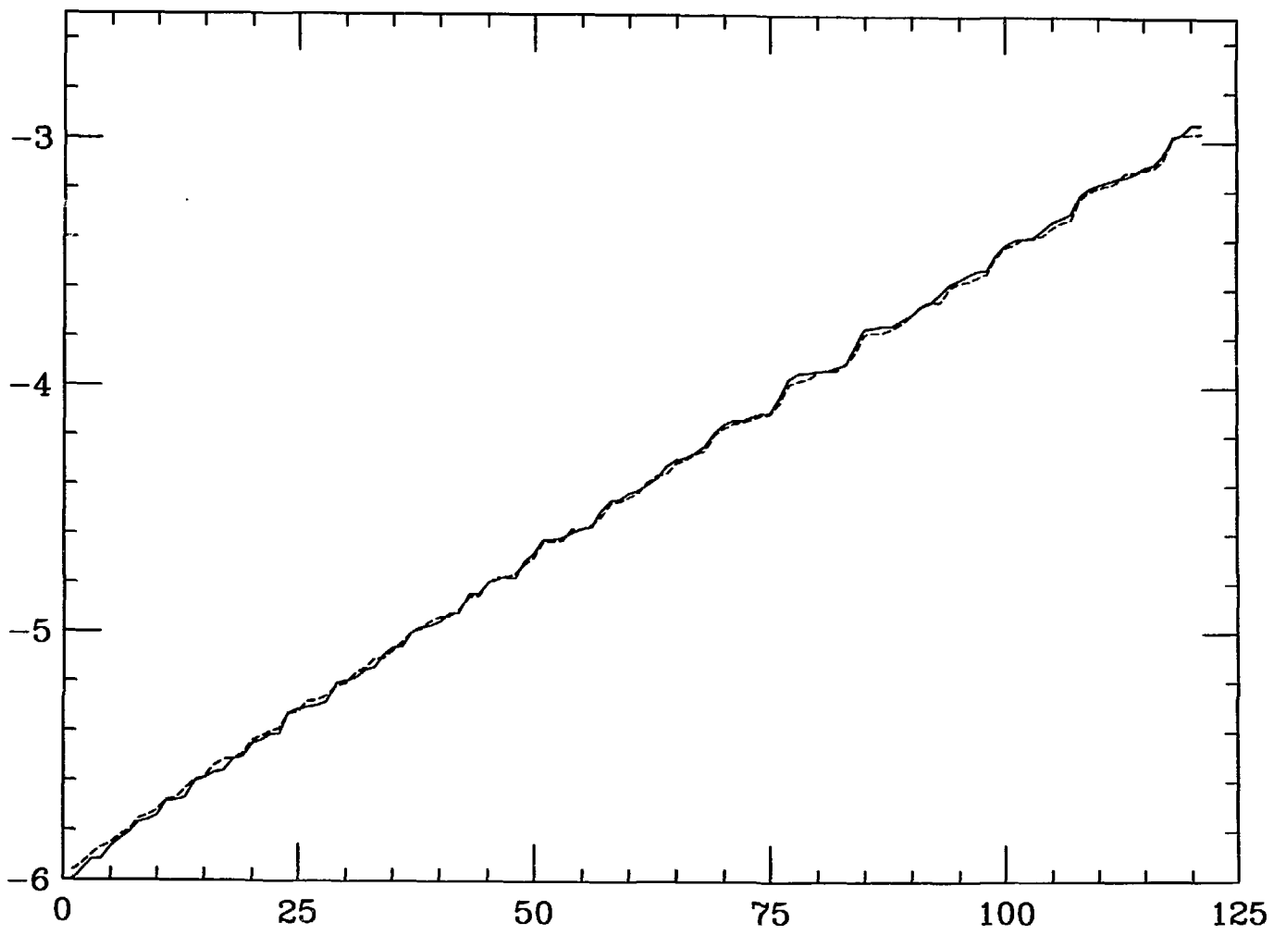
-3
-4
-5
-6
0
25
50
75
100
125

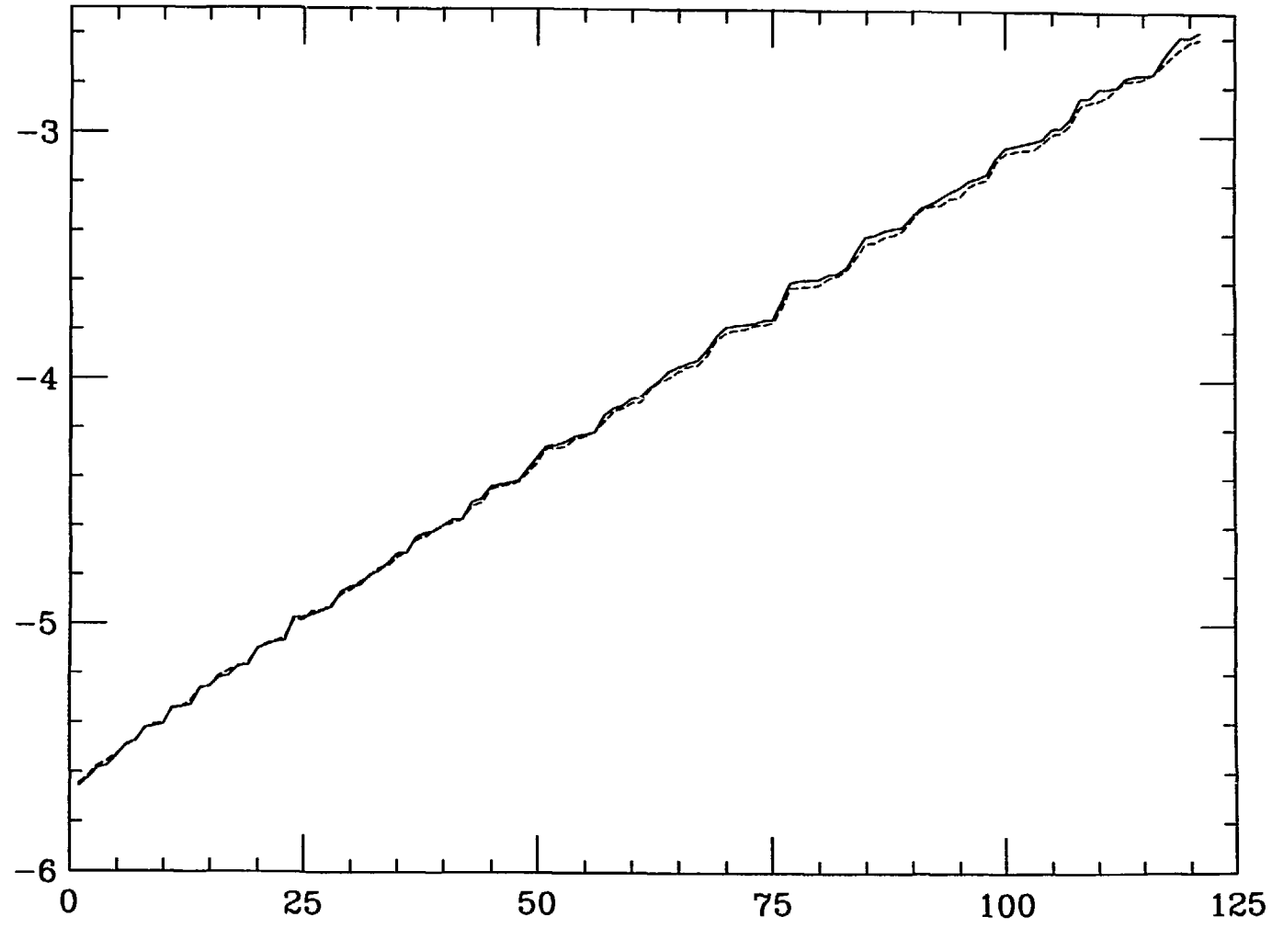
−3
−4
−5
−6
0
25
50
75
100
125

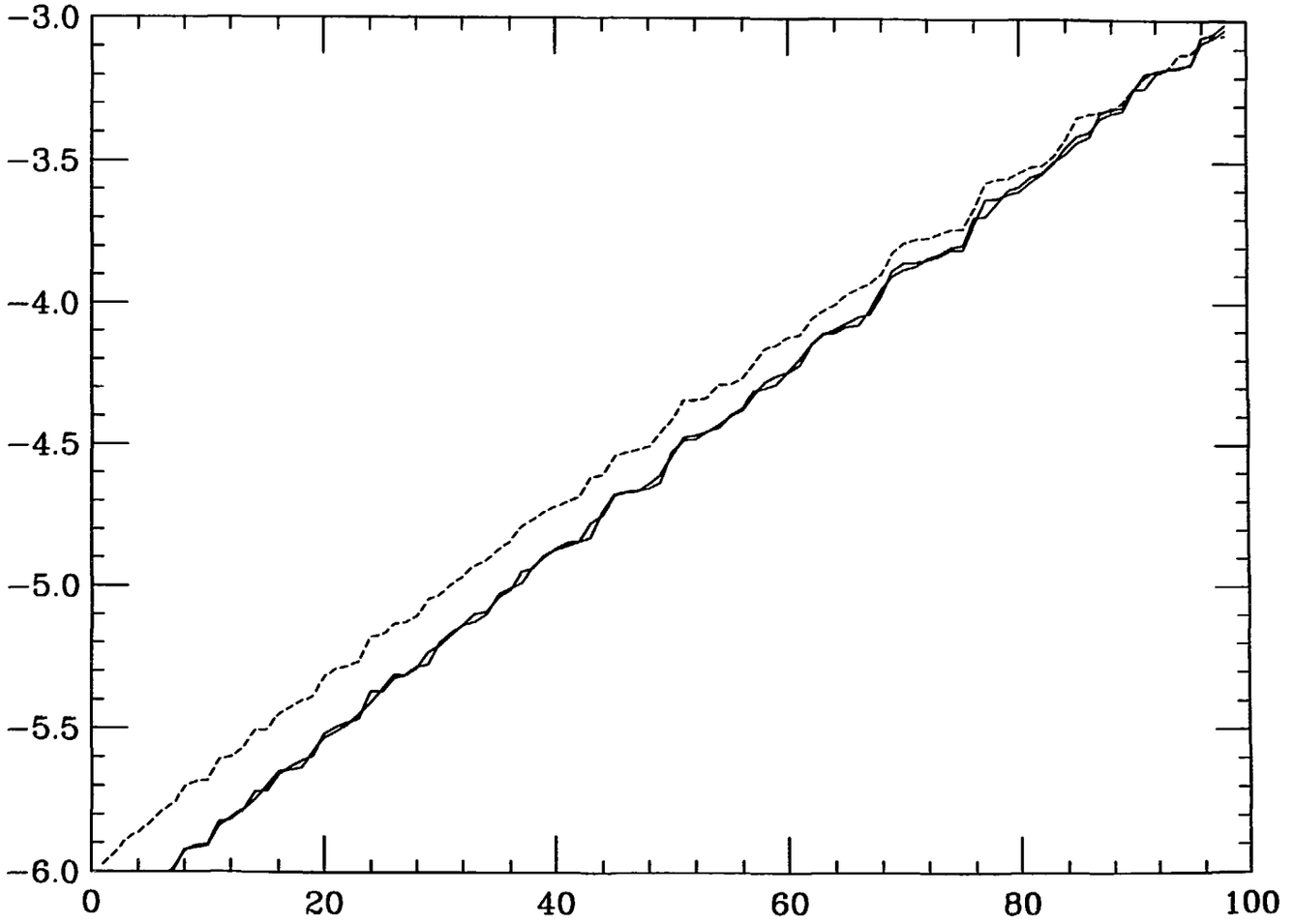
−3.0
−3.5
−4.0
−4.5
−5.0
−5.5
−6.0
0
20
40
60
80
100

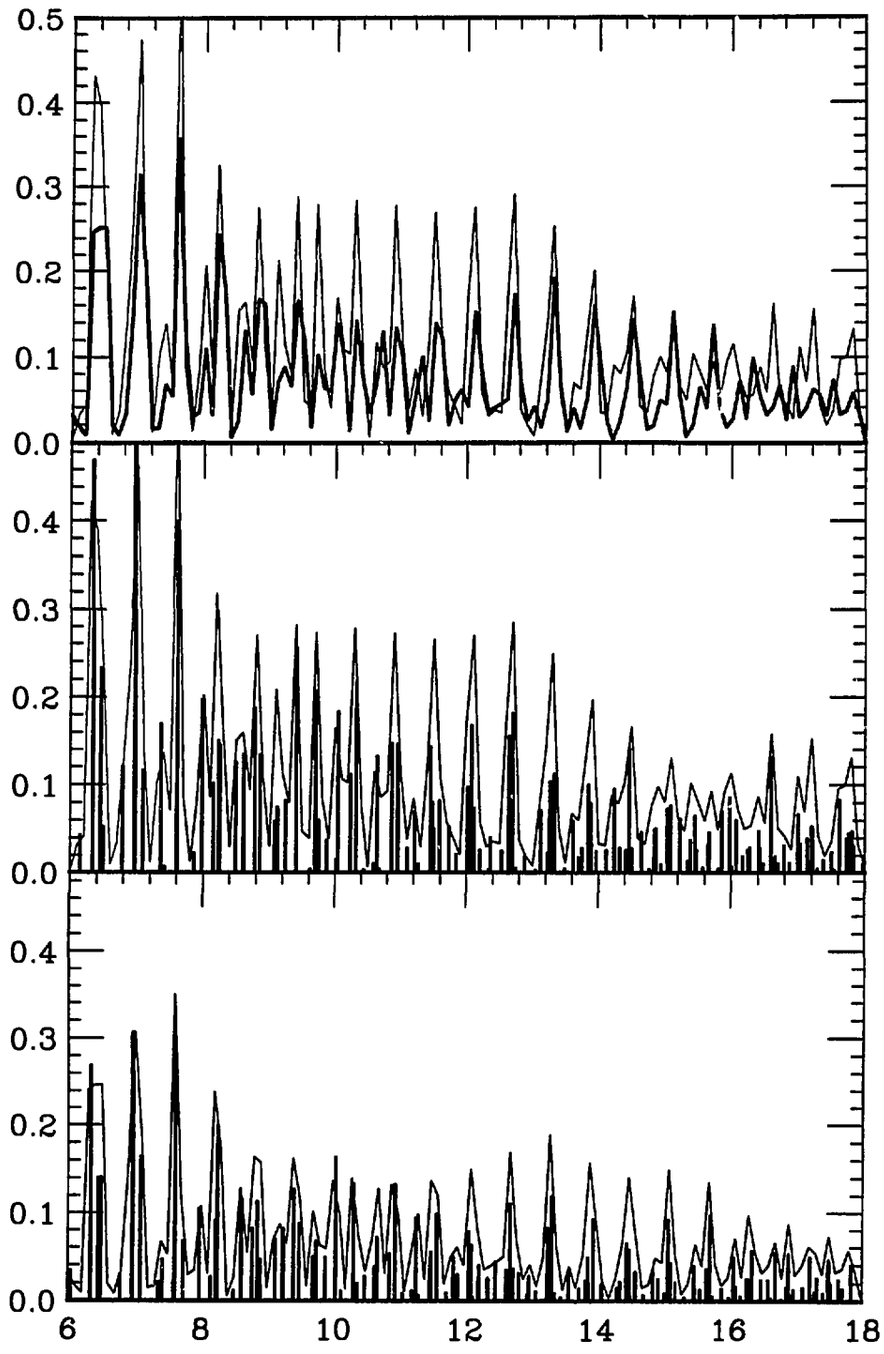
0.5
0.4
0.3
0.2
0.1
0.0
0.4
0.3
0.2
0.1
0.0
0.4
0.3
0.2
0.1
0.0
6
8
10
12
14
16
18

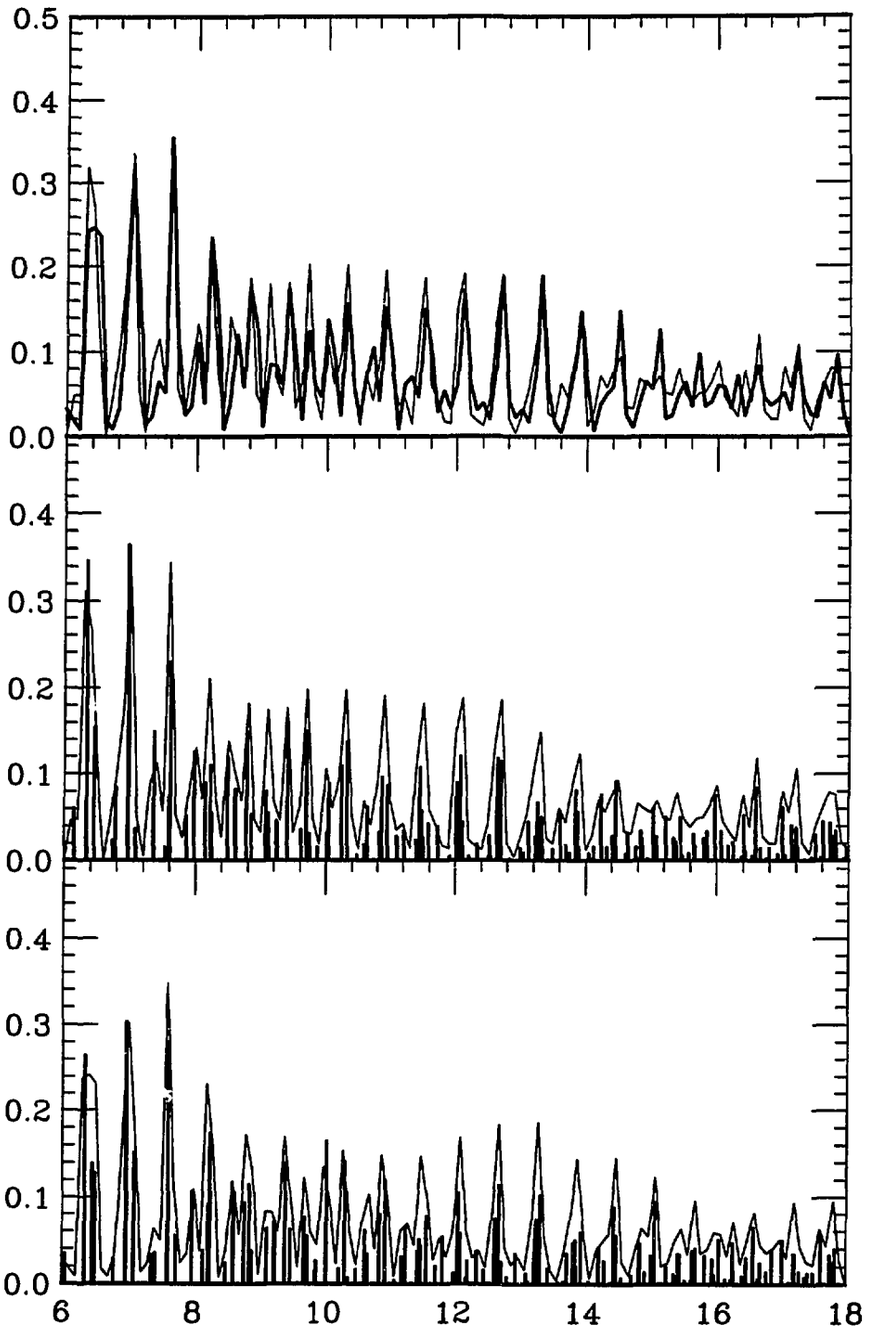
0.5
0.4
0.3
0.2
0.1
0.0
0.4
0.3
0.2
0.1
0.0
0.4
0.3
0.2
0.1
0.0
6
8
10
12
14
16
18

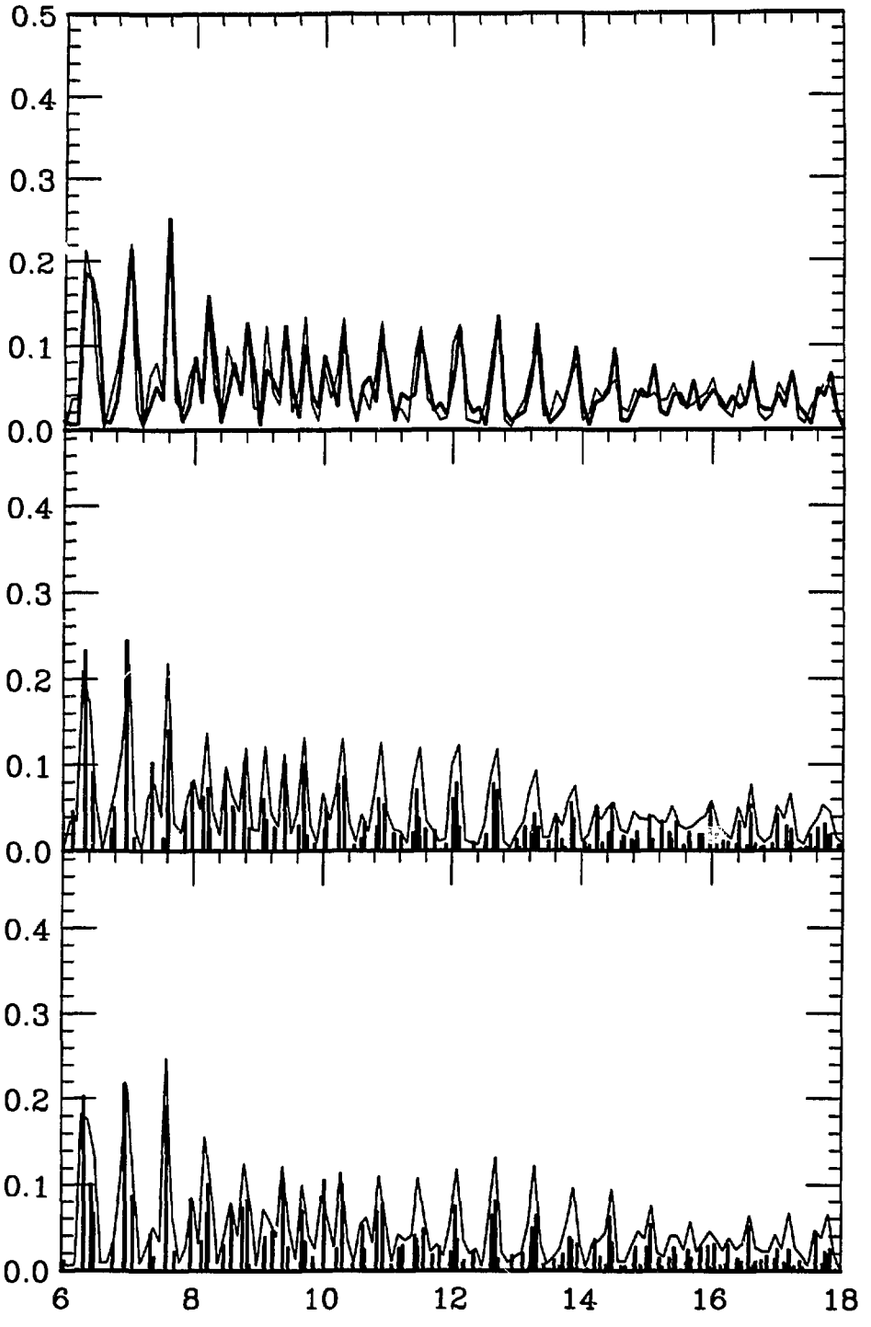
0.5
0.4
0.3
0.2
0.1
0.0
0.4
0.3
0.2
0.1
0.0
0.4
0.3
0.2
0.1
0.0
6
8
10
12
14
16
18

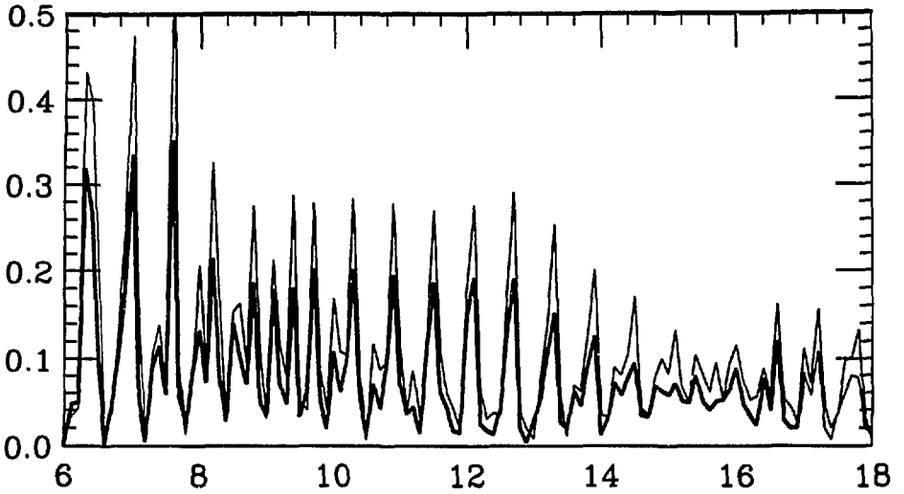
0.5
0.4
0.3
0.2
0.1
0.0
6
8
10
12
14
16
18

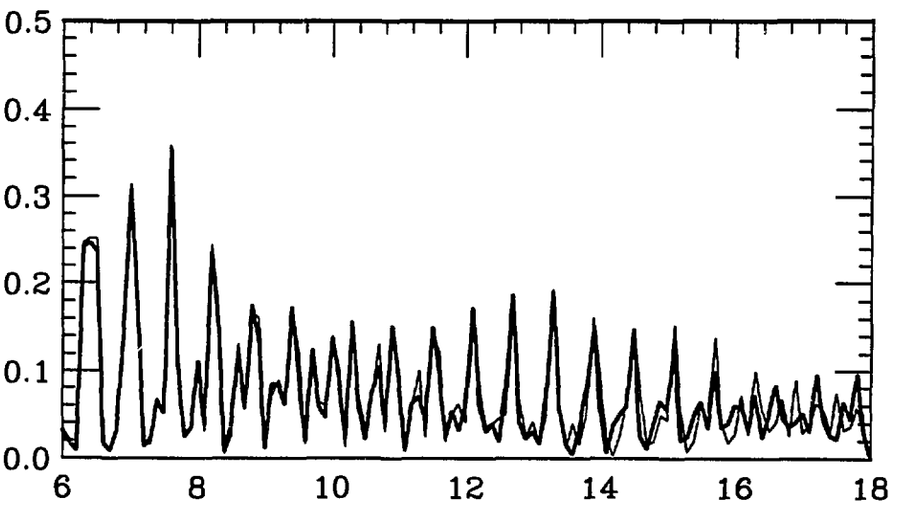
0.5
0.4
0.3
0.2
0.1
0.0
6
8
10
12
14
16
18

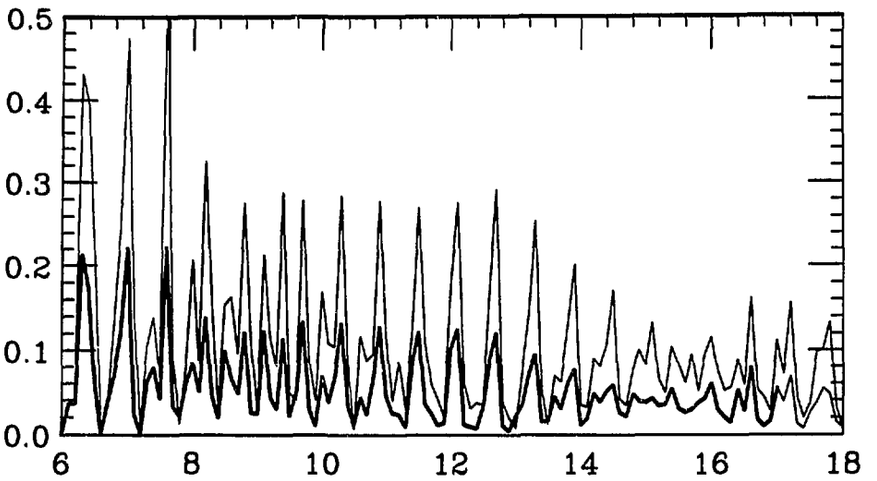
0.5
0.4
0.3
0.2
0.1
0.0
6
8
10
12
14
16
18

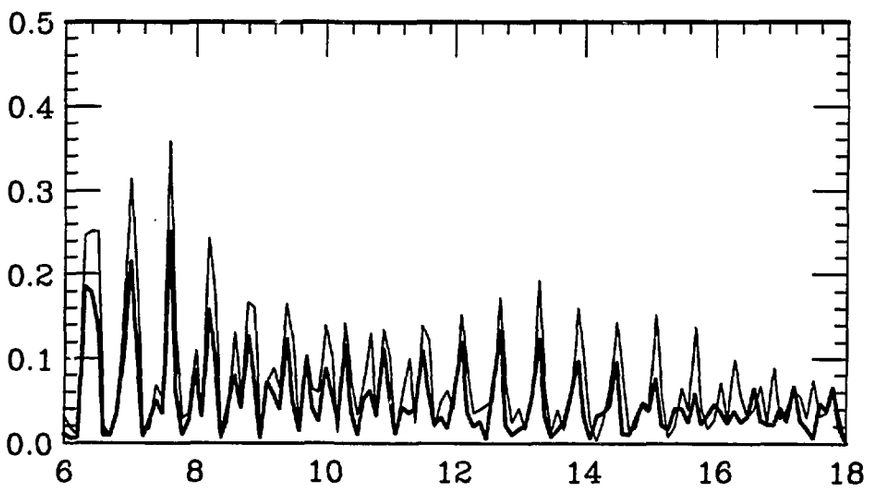
0.5
0.4
0.3
0.2
0.1
0.0
6
8
10
12
14
16
18

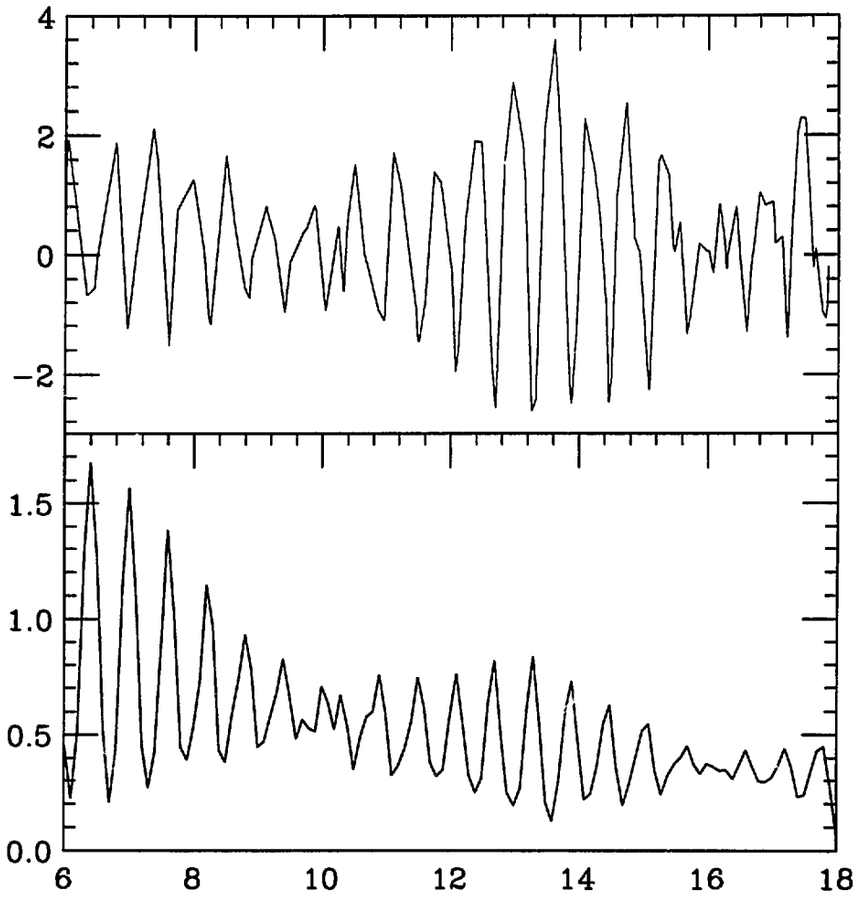
4
2
0
−2
1.5
1.0
0.5
0.0
6
8
10
12
14
16
18

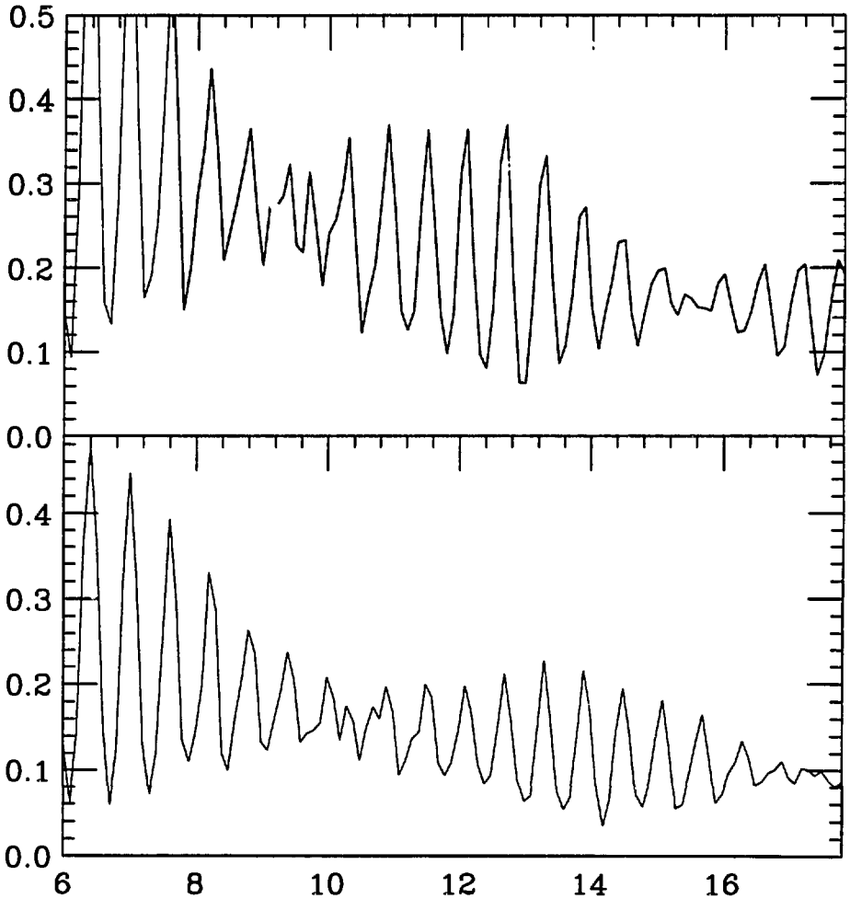
0.5
0.4
0.3
0.2
0.1
0.0
0.4
0.3
0.2
0.1
0.0
6
8
10
12
14
16